Supplement of Atmos. Chem. Phys., 23, 6559–6569, 2023
https://doi.org/10.5194/acp-23-6559-2023-supplement


Atmospheric Chemistry and Physics
Open Access

*Supplement of*

# Opposing trends of cloud coverage over land and ocean under global warming

**Huan Liu et al.**

*Correspondence to:* Ilan Koren (ilan.koren@weizmann.ac.il)

**Sect. S1. Spearman's correlation coefficient (Spearman's $\rho$)**

Spearman's $\rho$ is a nonparametric statistical measure of the strength of a monotonic relationship between two ranked variables. Spearman's $\rho$ ranges between -1 and 1, while 0 implies an absence of correlation, and proximity to ±1 $\rho$ values imply a stronger monotonic relationship. In this study, we calculate the Spearman's $\rho$ between different variables to measure their correlation. Since we are after correlations of interest in both negative and positive directions, we performed a two-tailed *t* test with a 95 % confidence interval ($p$ value < 0.05) to assess the statistical significance. For the computation of Spearman's $\rho$ and $p$ value, we used the Python library, *SciPy* (Version 1.5.2, https://scipy.org/, last access, 15 January).

**Sect. S2. A break in the annual global mean total cloud cover (TCC) series around 2000**

Our results reveal a clear break in the time series of the annual TCC, around the year 2000 as it can be observed in Fig. 2d in the Main Text. Here, we perform a more detailed analysis of this time series by separating it into the 3 analyzed domains: global, land and ocean. The results reveal that this break occurring around the year 2000 is mainly contributed by maritime clouds (blue curve in Fig. S1a), more specifically, those over the tropical Atlantic (oceans between 30° S–30° N and 110° W–22° E, Fig. S1c) and the western part of tropical Pacific (oceans between 30° S–30° N and 120° E–30° W, Fig. S1d).

The Atlantic Multi-decadal Oscillation (AMO) and Pacific Decadal Oscillation (PDO) are known to be the most active climate oscillations over the identified regions (Deser et al., 2010; Li et al., 2021), with a characteristic periodicity of decades, and were shown to have clear phase changes around the 2000s (Hong et al., 2022). Interestingly enough, over the Tropical Atlantic, the time series indicates an oscillation with a decreasing phase until ~1994 followed with an ascending phase for the next two decades, in consistency with the fingerprint of the AMO; while over the western Pacific, the sharp break observed over the years 2000–2001 may be attributed to the PDO.

This break in the time series of the mean annual TCC may affect locally the trend estimations over the Atlantic and western Pacific, but it is not likely to be the main driver of the trend mode as documented for the global TCC (see Figs. 4c–d in the Main Text). Indeed, one notices in Fig. 4c that the regions with larger anomalies are observed over land, the Indian Ocean, and the Eastern Pacific, while no obvious breaking is observed around year 2000 (in the corresponding time series shown in Figs. S1a, S1b, and S1e). In PC2 of the TCC and the annual global mean surface temperature (Fig. 4d in the Main Text), the 2000-breaking is present but to a lesser extent than in the TCC anomaly over the western Pacific (Fig. S1d) and actually contributes to the trend as many other local variations occurring over other time windows, supporting its unprevailing influence on the trend mode found in the Main Text.

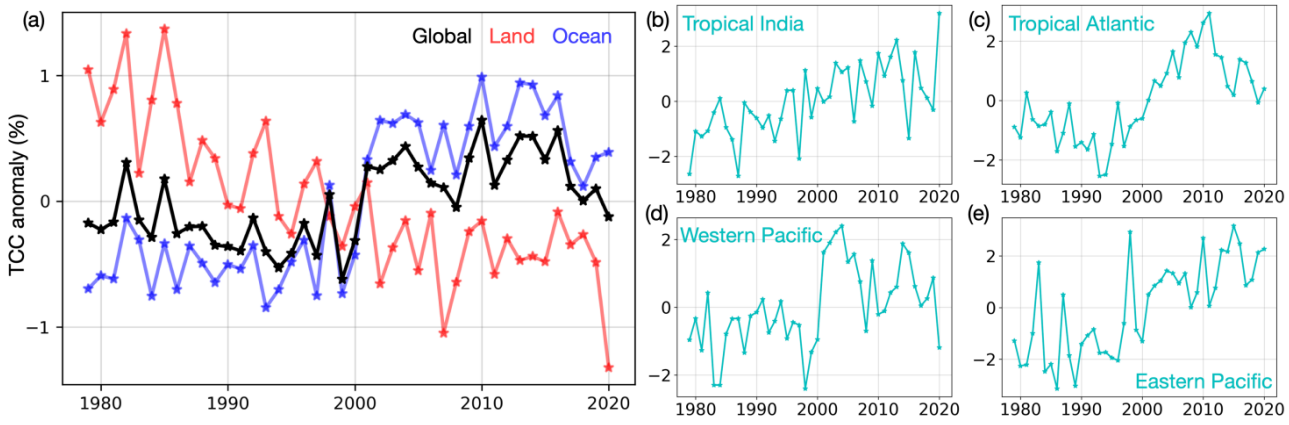


Figure S1: Time series of the anomaly of annual mean TCC over different regions, compared to the 1979–2020 average. TCC anomaly over the (a) global (black curve), land (red curve), and oceans (blue curve), (b) tropical India (oceans between 30° S–30° N and 22° E–120° E), (c) tropical Atlantic (oceans between 30° S–30° N and 110° W–22° E), (d) western Pacific (oceans between 30° S–30° N and 120° E–30° W), and (e) eastern Pacific (oceans between 30° S–30° N and 30° W–110° W)

**Sect. S3. Signal leakage analysis for the two dominant ST and TCC modes**

Additional analysis is performed to check signal leakage for the two dominant empirical orthogonal function (EOF) modes of the global surface air temperature (ST) and the global TCC that are shown in the Main Text. Figure S2 shows the histogram of explained variance for all the 42 EOF modes and their correlations with the two dominant EOF modes, as well as the correlations of the Principle Components (PCs) with the two dominant ones.

The explained variance by the first three EOF modes, in both ST (Fig. S2a) and TCC (Fig. S2d), is significantly larger than for the following modes. Moreover, the top two EOF modes (EOF1 and EOF2, Fig. S2b and S1e) and PCs (PC1 and PC2, Fig. S2c and S2f) for both ST and TCC show very weak correlations to other EOF modes and PCs. These results indicate that signal leakage is not a major problem in the interpretation of the dominant modes of ST and TCC, as discussed in the Main Text.

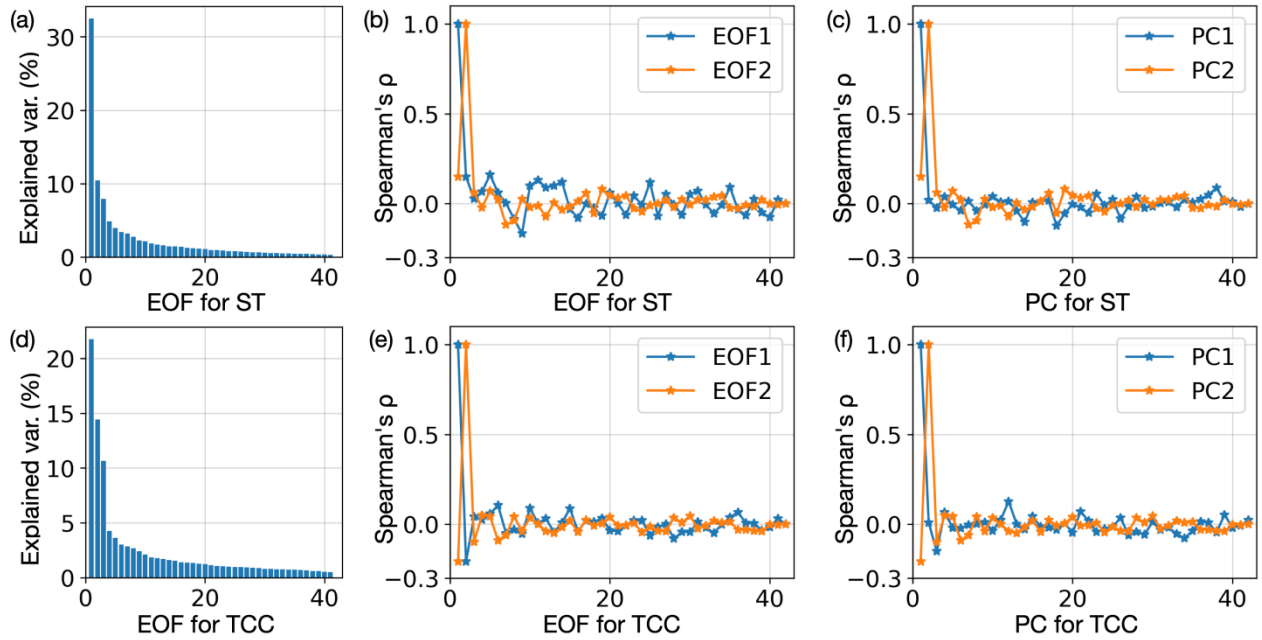


Figure S2: A signal leakage test for the top two EOF modes and PCs for ST and TCC. (a) Explained variance (unit: %) of all EOF modes for ST. (b) Correlations between the top two EOF modes and all EOF modes for ST. (c) Correlations between the top two PCs and all PCs for ST. (d–f) Same results as shown in (a–c), but for TCC.

**Sect. S4. Oceanic Niño Index (ONI)**

ONI is defined as the 3-month running mean of sea surface temperature anomaly over the Niño3.4 region (5° N–5° S and 170° W–120° W). It provides a common measure of the ENSO phases. Large positive ONI-values indicate strong warm phases of ENSO (El Niño, the unusual increase in sea surface temperature over the central and Eastern tropical Pacific Ocean), whereas large negative ONI-values correspond to strong cold phases of ENSO (La Niña, the cold counterpart of El Niño). Here, to link EOF modes for ST and TCC with known physical processes, such as ENSO, we calculate the ONI as the 3 month running mean of the monthly Niño-3.4 index obtained from the National Oceanic and Atmospheric Administration center for Weather and Climate Prediction (https://origin.cpc.ncep.noaa.gov/products/analysis_monitoring/ensostuff/ONI_change.shtml, last access, 30 March 2023).

**Sect. S5. Meteorological variables that correlate the second best with TCC**

To identify additional important meteorological factors driving the TCC variation besides the dominant ones discussed in the Main Text, we show in Fig. S3 the geographical distribution of the second-best parameters. These are the

meteorological variables that correlate best with the TCC, after excluding the best-correlated variable that is presented in Fig. 5b in the Main Text. It shows that over land, after relative humidity (RH), no additional, prominent variable stands out for strong correlations with continental TCC.

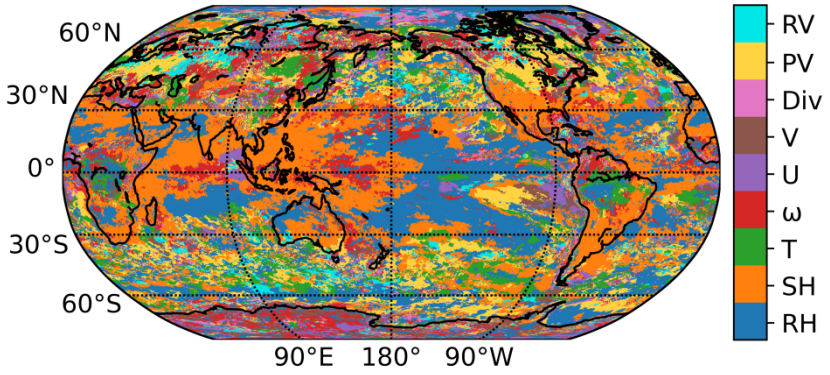


Figure S3: The ERA5 meteorological variables map that correlate the second best (variable, per gridbox, presented in Fig. 5b are not considered) with annual TCC data during 1979–2020. Spearman's ρ-values are calculated for annual RH, specific humidity (SH), temperature (T), U-wind component (U), V-wind component (V), wind divergence (Div), potential vorticity (PV), and relative vorticity (RV) at 23 standard pressure levels (1000, 975, 950, 925, 900, 875, 850, 825, 800, 775, 750, 700, 650, 600, 550, 500, 450, 400, 350, 300, 250, 225 and 200 hPa), respectively. Only Spearman's $\rho$ that are statistically significant at the level of 0.05 ($p$ value < 0.05, two-tailed $t$ test) are used.

**Sect. S6. $RH_{NS}$ trend significance and trend analysis of RH at 2 meters ($RH_{2m}$)**

Here, we explore the significance of estimated linear trends in near-surface RH ($RH_{NS}$) and trend maps of $RH_{2m}$ as complementary information to the results presented in the Main Text. Figure S4a presents a global picture of the $RH_{NS}$ trend (the same as Fig. 6a of the Main Text). Figure S4b presents only the significant values (the insignificant results are coloured as grey). As shown, most of the continental trends in $RH_{NS}$ are statistically significant and most maritime trends are statistically insignificant. Figures S4c and S4d present the results of the same analysis but for the $RH_{2m}$ (in %). Since $RH_{2m}$ is not provided by ERA5, per grid box and month, we calculated it using ST (in K) and dew point temperature at 2 meters ($Td_{2m}$, in K) according to the following formula (water surface is assumed):

$$RH_{2m} = 100 \times e^{17.502\left(\frac{Td_{2m}-273.16}{Td_{2m}-32.19}-\frac{ST-273.16}{ST-32.19}\right)}$$

The significance and similar continental patterns from this analysis further support the reduction in low-level RH as the most plausible explanation for the decreased continental cloud coverage, while other variables are likely to be responsible for changes in maritime cloud coverage.

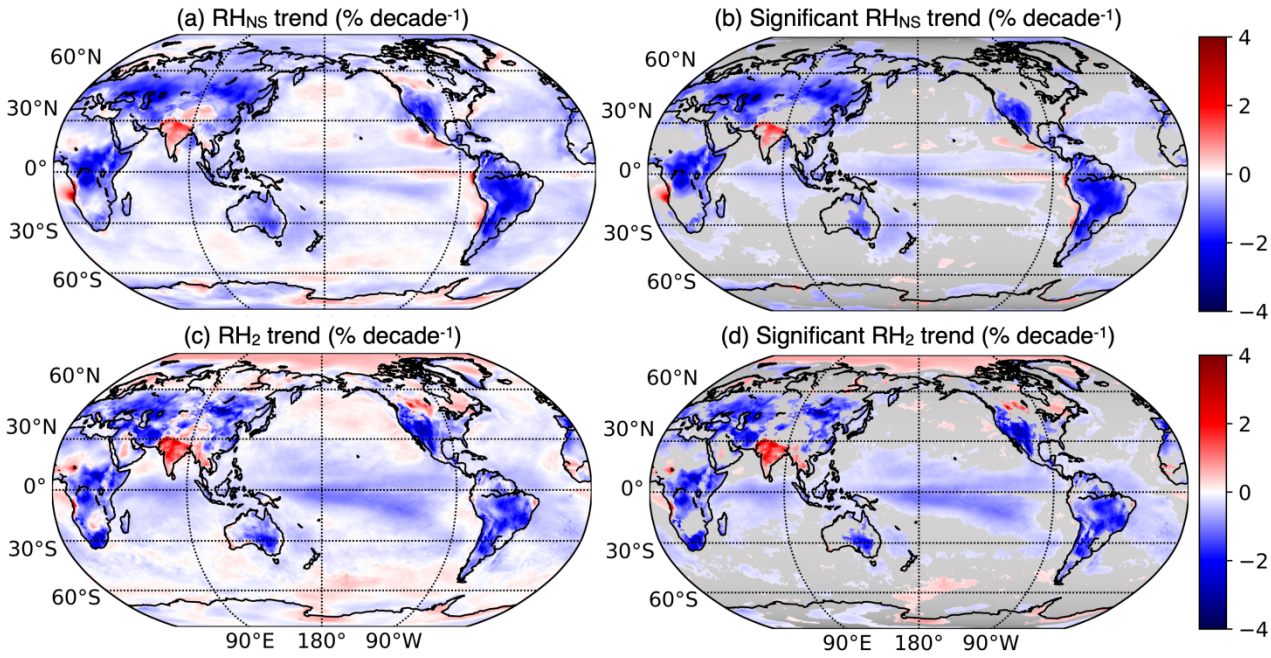


Figure S4: Trends in $RH_{NS}$ and $RH_{2m}$ during 1979–2020. (a) A map of global trend in $RH_{NS}$; (b) A map of $RH_{NS}$ trend that is statistically significant at the level of 0.05 ($p$ value < 0.05, two-tailed $t$ test); (c–d) the same as (a–b) but for $RH_{2m}$. The insignificant results are coloured in gray in panels (b) and (d).